arXiv:1108.5998v1 [physics.bio-ph] 30 Aug 2011

Equilibrium insertion of nanoscale objects into phospholipid bilayers

Sergey Pogodin, Vladimir A. Baulin†
Departament d'Enginyeria Quimica, Universitat Rovira i Virgili, Av. dels Paisos Catalans 26, 43007 Tarragona, Spain and †*ICREA, Passeig Lluis Companys 23, 08010 Barcelona, Spain**

Certain membrane proteins, peptides, nanoparticles and nanotubes have rigid structure and fixed shape. They are often viewed as spheres and cylinders with certain surface properties. Single Chain Mean Field theory is used to model the equilibrium insertion of nanoscale spheres and rods into the phospholipid bilayer. The equilibrium structures and the resulting free energies of the nano-objects in the bilayer allow to distinguish different orientations in the bilayer and estimate the energy barrier of insertion.

I. INTRODUCTION

Biological membranes protect cells against the environment and also provide for selective transport of nanoscale objects across the membranes[1]. Peptides, nanotubes, nanoparticles and other nano-objects with fixed shape can interact with phospholipid bilayers[2], accumulate inside the membranes[3] and penetrate into cells[4–6]. Surface activity of these objects raises issues of biocompatibility and cytotoxicity[7,8], which may limit their biomedical applications. Understanding and controlling the interactions of nanoscale objects with membranes is therefore a key to the design of novel medical treatments and cell-active substances which can modulate the thermodynamic properties of cell membranes.

Although membrane active peptides, membrane proteins, nanotubes and nanoparticles may significantly differ in composition and chemical structure, the membrane activity implies the presence of certain common features providing for such activity. Phospholipid bilayers have alternating hydrophilic and hydrophobic regions which are characterized by the corresponding thickness. Thus, the size and the shape of nanoscale objects need to be compatible with the bilayer structure to ensure their insertion into the bilayer (*e.g.* the concept of hydrophobic matching[9]), cell penetration[10,11] or pore formation[12,13]. The thickness of the hydrophobic core defines the length scale for the size while the planar geometry of the bilayer defines the template for the shape of nanoscale objects able to interact or insert into phospholipid bilayers. The effect of the shape of nanoparticles interacting with phospholipid bilayers have been studied in Ref.[14]. The nanoparticles-lipid bilayer interaction is determined by the contact area and the local curvature of the nanoparticle at the contact point with the bilayer. Thus, nanoscale objects of different nature can be viewed in the first approximation as geometrical objects described only by the shape and the surface properties[14–18].

Many theoretical studies of interaction of phospholipid bilayers with nanoparticles and even peptides consider the simplest shapes: a sphere[3,19–21] and a cylinder[18,22–26]

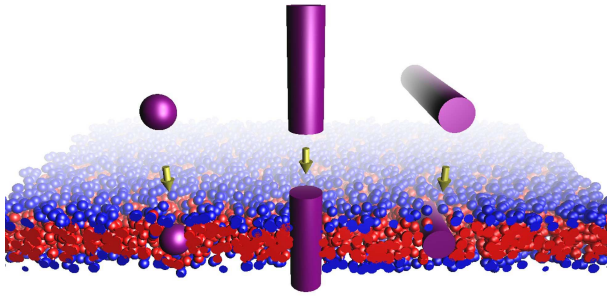

FIG. 1. Three geometries of nanoscale objects considered in the text: insertion of a sphere (left), insertion of a perpendicular cylinder (middle), and insertion of a parallel cylinder (right) into the bilayer.

with uniform or patterned surface properties. This allows to describe a broad range of objects of similar size within a single concept and provide a general picture on the mechanism and the molecular details of interaction with the bilayers. Coarse-grained Molecular Dynamics (MD) provides the most detailed information about the molecular structure and the dynamics of interaction of nanoscale objects with phospholipid bilayers[3,14,18,19,23,27–31]. However, this method becomes computationally expensive and time consuming when the size of the system and the number of interacting molecules increases[32]. Calculation of equilibrium properties and equilibrium free energies requires equilibration process which may exceed microseconds[32]. One of the alternatives is the use of the self-consistent field theories, where the equilibrium structure of the bilayer is found from the solution of the self-consistency equations. Recently, Single Chain Mean Field (SCMF) theory has been applied for modeling of the phospholipid bilayers at different levels of coarse-graining[33]. It was shown, that essential equilibrium properties of the phospholipid bilayer such as the thickness, position of different groups, the compressibility constant and the area per lipid, can be reproduced with high accuracy. High speed of calculations is obtained by the decoupling of the correlations between the molecules and the fluctuations, taking into account the symmetries in the system. In this manner, the multi-molecule problem is reduced to a single molecule in the external self-consistent

* vladimir.baulin@urv.cat

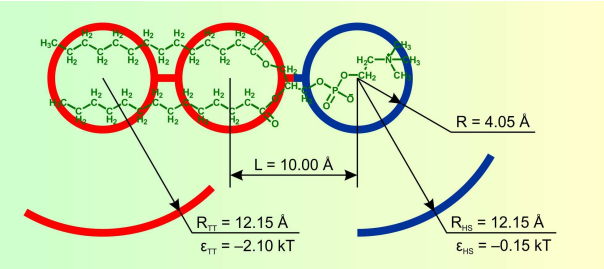

FIG. 2. The 3-beads model of the DMPC phospholipid molecule. R is the radius of the hydrophobic T-beads (red) and hydrophilic H-bead (blue), L is the bonds length, R_{TT} and R_{HS} are the interaction radii of the corresponding stepwise attractive potentials.

field problem. The molecule conformations and the fields are found from the self-consistency condition and gives the free energy of the equilibrium structures as a result of calculations. This method has been applied to estimate the free energies of insertion of a carbon nanotube into a phospholipid bilayer[22] and to elucidate the patterning of a carbon nanotube for physical translocation through the bilayer[34].

In this publication, we first present equations of the SCMF theory for the interaction of phospholipid bilayer and nanoscale objects. This theory is then applied for calculation of equilibrium structures and free energies of resulting structures of phospholipids and nanoscale objects, modeled as spheres and cylinders with given surface properties (Fig. 1).

II. THEORY

The SCMF theory uses a coarse-grained representation of a phospholipid molecule as a set of spherical beads interacting with the fields through simple effective potentials[33]. The simplest 3-beads model (Fig. 2) is able to reproduce with high accuracy the equilibrium structure and properties of DMPC phospholipid bilayer, such as the average interfacial area per lipid, the thickness of the bilayer and the core, and the stretching modulus[33]. In this model the phospholipid molecule is represented by two hydrophobic beads (T) and one hydrophilic bead (H) of the same radius 4.05 Å, joined consequently by rigid bonds of length 10.0 Å, and able to bend around the central T-bead. Two T-beads, belonging to different molecules, interact with energy gain $\epsilon_{TT} = -2.10$ kT at distances between their centers smaller than 12.15 Å. Additionally, the H-beads interact with implicit solvent molecules, assumed as well to be represented by spherical beads of the same radius 4.05 Å, with energy gain $\epsilon_{HS} = -0.15$ kT at the distances closer than 12.15 Å.

The free energy of a system, containing N lipid molecules and the solvent, depends in general on the total probability distribution function ρ of the system. In the mean field approximation one can split this multi-molecule probability distribution function into a product of the corresponding single-molecule distribution functions. This allows to write the total free energy of the 3-beads model as a sum

$$F = -S_L - S_S + U_0 + U_{TT} + U_{HS} + U_{steric} \quad (1)$$

where S_L and S_S are the entropy contributions of the lipids and the solvent, U_0 describes the intra-molecular and position-dependent energies of the lipids, U_{TT} and U_{HS} represent the inter-molecular interactions between the pairs of T-beads and between H-beads and the solvent, and the last term, U_{steric}, takes into account the hard-core steric repulsions between the molecules.

The entropy part of the free energy is written as

$$-S_L - S_S = N \langle \ln [\rho(\gamma) N \Lambda] \rangle + \int c_S(\boldsymbol{r}) \ln [c_S(\boldsymbol{r}) \Lambda_S] \, d\boldsymbol{r} \quad (2)$$

where $\rho(\gamma)$ is the density of probability of a single lipid molecule to be in the conformation γ (along with relative positions of the beads in the molecule with respect to each other, the conformations also include their spatial position and orientation in the system), $c_S(\boldsymbol{r})$ is the solvent concentration at the point $\boldsymbol{r}$, Λ and Λ_S are the de Broglie lengths for the lipids and the solvent respectively, which shift the absolute value of the free-energy but have no effect on the final results. The angular brackets denote the average over $\rho(\gamma)$, and the integral is taken over all the accessible volume of the system.

The intra-molecular interaction energy U_0 is simply the average over $\rho(\gamma)$

$$U_0 = N \langle U_0(\gamma) \rangle \quad (3)$$

where $U_0(\gamma)$ is the internal energy of the lipid molecule in the conformation γ. It can include interactions between the beads composing the molecules and interaction with the external fields and the walls (or impermeable immobile objects).

The combined inter-molecular energy terms are written as

$$U_{TT} + U_{HS} = \frac{N(N-1)}{2} \int \langle u_T(\gamma, \boldsymbol{r}) \rangle \langle c_T(\gamma, \boldsymbol{r}) \rangle \, d\boldsymbol{r} + N \int \langle u_S(\gamma, \boldsymbol{r}) \rangle c_S(\boldsymbol{r}) d\boldsymbol{r} \quad (4)$$

where $u_T(\gamma, \boldsymbol{r})$ and $u_S(\gamma, \boldsymbol{r})$ are the interaction potentials for T-beads and the solvent at the point $\boldsymbol{r}$, created by the lipid molecule in the conformation γ, and $c_T(\gamma, \boldsymbol{r})$ is the concentration of T-beads of the lipid in conformation γ at the point $\boldsymbol{r}$.

5 is valid only if the potentials $u_T(\gamma, \boldsymbol{r})$ and $u_S(\gamma, \boldsymbol{r})$ are finite and smooth functions of $\boldsymbol{r}$ and therefore cannot contain any hard-core steric repulsion interactions, which are included in a separate term, U_{steric}, representing the incompressibility condition at every point $\boldsymbol{r}$ of the system

$$U_{steric} = \int \lambda(\boldsymbol{r}) \left(\phi_0 - v_S c_S(\boldsymbol{r}) - N \langle \phi(\gamma, \boldsymbol{r}) \rangle \right) d\boldsymbol{r} \quad (5)$$

Here $\lambda(\boldsymbol{r})$ is the Lagrange multiplier and ϕ_0 is the total volume fraction occupied by the lipids and the solvent ($0 < \phi_0 < 1$), v_S denotes the volume of the solvent molecule, and $\phi(\gamma, \boldsymbol{r})$ is the volume fraction at the point $\boldsymbol{r}$ occupied by the lipid in the conformation γ.

To find the equilibrium distribution, one should minimize the total free energy (1) with respect to $\rho(\gamma)$ and the solvent distribution $c_S(\boldsymbol{r})$ subject to the incompressibility condition (5). The minimization leads to the following set of integral equations

$$\rho(\xi) = \frac{1}{Z} \exp\left[-U_0(\xi) - (N-1)\int u_T(\xi,\boldsymbol{r})\,\langle c_T(\gamma,\boldsymbol{r})\rangle\, d\boldsymbol{r} - \int u_S(\xi,\boldsymbol{r}) c_S(\boldsymbol{r}) d\boldsymbol{r} + \int \lambda(\boldsymbol{r})\phi(\xi,\boldsymbol{r}) d\boldsymbol{r}\right] \quad (6)$$

$$v_S\lambda(\boldsymbol{r}) = \ln\left[v_S c_S(\boldsymbol{r})\right] + N\,\langle u_S(\gamma,\boldsymbol{r})\rangle \quad (7)$$

$$v_S c_S(\boldsymbol{r}) = \phi_S(\boldsymbol{r}) = \phi_0 - N\,\langle \phi(\gamma,\boldsymbol{r})\rangle \quad (8)$$

where the normalization factor Z ensures that $\int \rho(\gamma) d\gamma = 1$. These equations can be solved numerically, if the integrals and the averages are replaced by appropriate sums, which reduce the problem to solution of algebraic equations. To discretize the space, the simulation box is divided into a set of auxiliary cells, where all spatial dependent variables have a constant value. The division into cells should also take into account the symmetry of the solution, which provides the speed up of the calculations. For example, if the lipid system is expected to self-organize into a flat bilayer, the division of the simulation box according to 1D geometry into parallel slits results in considerably smaller number of cells than the 3D division into a cubic grid with the same resolution. The conformational space γ of a single lipid is sampled with the Rosenbluth algorithm[35], the conformations are placed in the box and the spatial distributions $u_T(\gamma,\boldsymbol{r})$, $u_S(\gamma,\boldsymbol{r})$, $c_T(\gamma,\boldsymbol{r})$, $\phi(\gamma,\boldsymbol{r})$ as well as other necessary conformational-dependent properties are calculated. Finally, the averages of the fields f in the equations 6-8 are replaced by the sums

$$\langle f(\gamma)\rangle = \frac{1}{\kappa}\sum_{\gamma}\frac{\rho_\gamma f_\gamma}{w_\gamma} \quad (9)$$

where f_γ is the value of this field, and ρ_γ is the probability of the conformation γ belonging to the generated sampling (thus ρ_γ is determined only over the sampling, while $\rho(\gamma)$ used above was determined in the full conformational space of the molecule). w_γ is the value of the Rosenbluth weight (*i.e.* biased probability of the conformation γ is introduced into the sampling during the generation). κ is the size of the conformational sampling. Similarly, the integrals over the space are replaced by the sums as

$$\int f(\boldsymbol{r}) d\boldsymbol{r} = \sum_i f_i V_i \quad (10)$$

where f_i is the value of the field in the i-th auxiliary cell of the simulation box and V_i is the volume of the i-th cell. As a result, the system of integral equations 6-8 is reduced to the closed set of algebraic equations of finite but huge number κ of unknown variables ρ_γ. Since the larger κ, the more accurate the solution is, the practical choice of κ which provide a reasonable accuracy is limited by the *representative* sampling. The easiest way to check the accuracy is to perform several simulations with independently generated random samplings and compare their results. Thus we start our simulations with some small value of κ, and then perform series of similar simulations for larger κ till the moment when further increase of κ will not lead to significant change of calculated results. For the simulations reported in this work we used $\kappa = 750000$, which provide accuracy of the calculated energies about ± 10 kT.

The number of auxiliary cells in the box should be high enough to provide acceptable spatial resolution, but if it is relatively small one can decrease the number of independent variables by introducing new independent variables, average concentration of T-beads, $c_{T,i} \equiv \langle c_T(\gamma,\boldsymbol{r}_i)\rangle$, potential of the solvent, $u_{S,i} \equiv \langle u_S(\gamma,\boldsymbol{r}_i)\rangle$, and the volume fraction occupied by lipids, $\phi_i \equiv \langle \phi(\gamma,\boldsymbol{r}_i)\rangle$. Depending on the method of solution of equations[1], such reduction of the number of independent variables can speed up calculations.

The equations of the SCMF theory are written for the canonical (NVT) ensemble. However, the simulation of the phospholipid bilayer with inserted nanoscale object would require the grand-canonical ensemble, since the inserted object may expel the phospholipids out of the simulation box. Fortunately, the SCMF technique is fast enough to perform series of canonical calculations for a part of bilayer with variable number of lipids N in the simulation box. One can consider then the simulation box as an open part of a larger closed system and thus estimate the free energy F^* of the whole system as a function of N. The equilibrium value of N will correspond to the minimum of F^*, thus series of canonical SCMF calculations are equivalent to a grand-canonical

[1] According to Ref.[33], the independent variables are $c_{T,i}$, $c_{H,i}$ and ϕ_i. One can show that the expression $N\,\langle u_S(\gamma,\boldsymbol{r})\rangle$, which is the average potential experienced by the solvent molecule at the point $\boldsymbol{r}$, is approximately equal to $N\epsilon_S\,\langle c_H(\gamma,\boldsymbol{r})\rangle$, where ϵ_S is the integral of the H-S interaction potential around a solvent molecule. One can easily replace the variables $u_{S,i}$ by $c_{H,i}$. This was indeed necessary in the general case, considered in the previous article, but in this context it can be avoided for the sake of simplicity.

calculation. In the simulations performed in the present work (size of the system about $100.0 \times 100.0 \times 60.0$ Å, two-dimensional geometry with spatial resolution 2.0 Å, and sampling size $\kappa = 750000$), calculation of one energy point in the grand-canonical ensemble with current version of our SCMF code, demanded, on average, about one day on a 32-cores machine. Full three-dimensional simulations should be significantly slower, but we believe that further improvements of our code will significantly speed-up its' performance, thus making possible three-dimensional simulations in a reasonable time.

III. RESULTS AND DISCUSSION

The equations of the previous section allow to calculate the equilibrium properties and the free energy of the phospholipid bilayer and its interaction with nanoscale objects with a fixed shape. Simulation of a phospholipid bilayer is a one dimensional problem if we neglect the bilayer bending. Since the free energy of a homogenous bilayer is proportional to the area (or the number of lipids in the bilayer) and the interfacial area per lipid and the bilayer thickness are constant along the bilayer, the free energy of a large system F^* can be written as

$$F^* = V^* f_S + N^* f(A), \quad f(A) = \frac{F(V,N,A) - V f_S}{N}, \quad f_S = \frac{\phi_0}{v_S} \ln \frac{\phi_0}{v_S} \tag{11}$$

where V^* is the volume and N^* is the total number of lipids of the large system, f_S is the free energy density of the region occupied by the pure solvent, and $f(A)$ is the free energy per lipid of the bilayer, which depends on the average surface area per lipid A.

The result of the SCMF simulation is the free energy $F(V,N,A)$ of the box of the total volume V with the number of lipids N. These expressions allow to construct the free energy per lipid $f(A)$. The equilibrium area per lipid A_0, which minimizes the total free energy of a large system F^*, can be found by the minimization of $f(A)$, obtained from the series of SCMF simulations, while the simulation corresponding to A_0 gives the equilibrium distribution of T- and H-beads inside the bilayer and the equilibrium thickness (Fig. 3).

Similar approach is applied to study the insertion of a rigid spherical or cylindrical nano-object into the phospholipid bilayer. A part of the object located inside the simulation box is represented by a region prohibited for lipids and the solvent to enter, and the surface of the object can interact preferentially with phospholipid beads. This restricted area is taken into account during the sampling generation by the additional bias and the corresponding contribution to the intra-molecular energy $U_0(\gamma)$. In the case of a spherical object and a cylindrical object oriented perpendicular to the bilayer one can use the two-dimensional cylindrical geometry with the symmetry axis passing through the center of the sphere (cylinder) perpendicular to the bilayer plane. The simulation of a cylindrical object in the parallel orientation has been done within two-dimensional grid geometry *i.e.* assuming infinite cylinder. To limit the bending of the bilayer, which permits the inserted object to escape from the bilayer, the hard walls on the top and bottom of the simulation box have been introduced. Assuming that a part of the membrane outside the simulation box is not perturbed by the insertion of the object and, thus, is in equilibrium state, we estimate the total free energy change due to the insertion of the object to a given position $\boldsymbol{p}$ in the box as

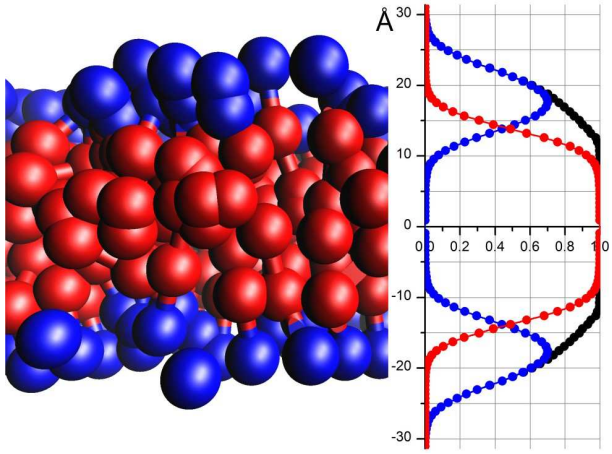

FIG. 3. Mean field snapshot of DMPC bilayer at equilibrium within the 3-beads model (left), and the corresponding concentration profiles (right) of hydrophobic (red), hydrophilic (blue) and total (black) volume fractions of the beads.

$$\Delta F^* = F(V,N,\boldsymbol{p}) - N f(A_0) - (V - V(\boldsymbol{p})) f_S \tag{12}$$

where $F(V,N,\boldsymbol{p})$ is the free energy of the box and $V(\boldsymbol{p})$ is the volume occupied by the object inside the box.

The results of the free energy calculations for spheres and cylinders of diameter 2.43 nm with homogeneous surface properties are summarized in Fig. 4. The surface properties are described by a single interaction parameter between the T-beads and the surface, ϵ. One can clearly see, that the free energy changes due to the insertion of a sphere, or a cylinder in perpendicular orientation which has a similar contact area with lipids, have relatively close values for all considered levels of hydrophobicity ϵ. Thus, the shape of the object is not so important as the contact area with lipids. This conclusion is consistent with the previous observations[14]. In contrast, the cylinder in the parallel orientation has a larger contact area with phospholipid tails and disturbs much larger part of the bilayer. Thus, the parallel orientation has sufficiently lower equilibrium free energy than the perpendicular orientation (the points in the plot correspond to a cylinder with the length 10.0 nm, while the numbers in the insets correspond to the energy per nm).

Hydrophilic and hydrophobic objects induce different rearrangement of lipids in the bilayer (see the insets of

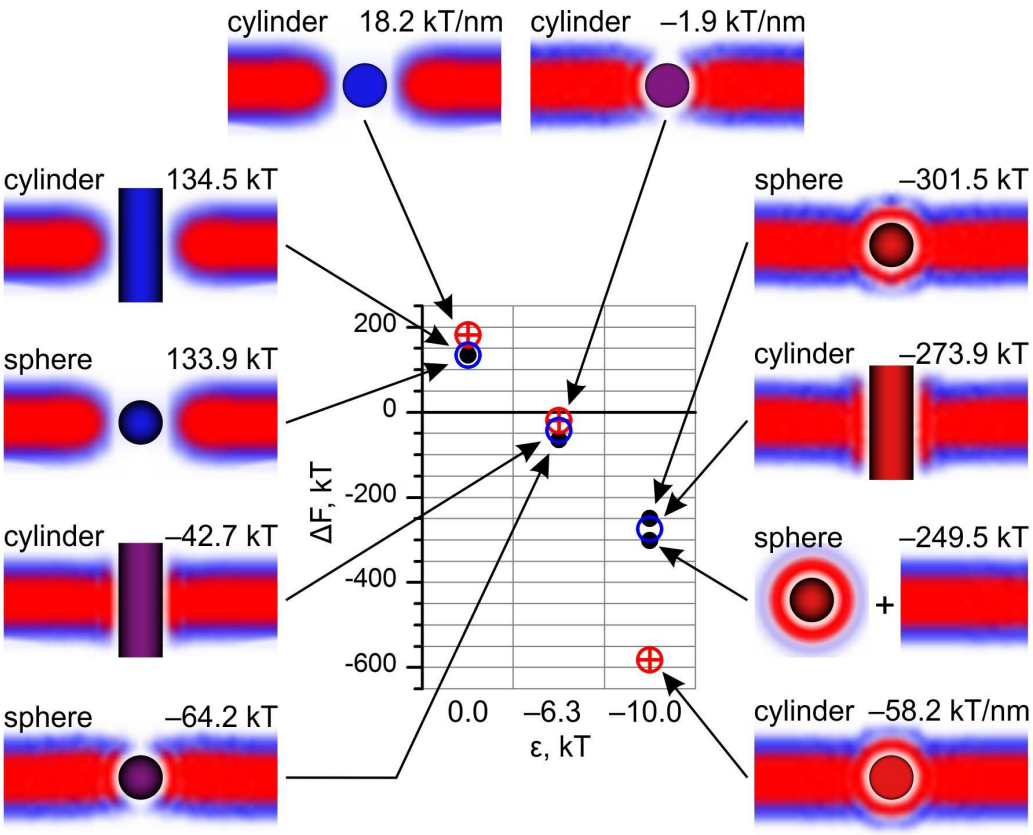

FIG. 4. Snapshots of the equilibrium insertion of a spherical and a cylindrical object into the DMPC bilayer. The color of the objects in the insets illustrates the hydrophobicity level (interaction with T-beads): $\epsilon = 0.0$ (blue), $\epsilon = -6.3$ kT (purple), $\epsilon = -10.0$ kT (red). Parallel orientation of a cylinder (denoted by the energy/nm), corresponds to the cylinder of length 10.0 nm.

Fig. 4). Hydrophilic objects of similar size create pores of similar size with the heads of the lipids oriented inside the pores. Hydrophobic objects attract the tails of phospholipids and they tend to come closer to the surface. For most hydrophobic objects, the meniscus provoked by the wetting of the hydrophobic object can be formed. For intermediate interaction parameters, the pore is not complete and is combined with the partial wetting at the edges, thus provoking the thinning of the bilayer in contact with the nano-object. This diagram also suggest the preferential orientation of cylindrical objects in the bilayer. Hydrophilic cylinder has lower free energy in perpendicular orientation, while the most hydrophobic cylinder has lower free energy in parallel orientation. For an intermediate hydrophobicity, there is a transition in orientation from perpendicular to parallel orientation which depends also on the length of the cylinder. For $\epsilon = -6.3$ kT the transition from perpendicular to parallel orientation occurs at the length of the cylinder 10 nm, where both orientations have almost the same energies. Longer cylinders would favor parallel orientation.

The uptake of a hydrophobic particle into the core of a bilayer is not the only equilibrium solution of the equations. There exists a solution which corresponds to a hydrophobic particle covered by phospholipids floating around and coexisting with a bilayer (third snapshot from the top in the right column of Fig. 4). We have compared the free energy of such structure with the energy of the inserted sphere into the bilayer in the most hydrophobic case, $\epsilon = -10.0$ kT. The bilayer with the incorporated sphere has a lower energy, while the free energy difference with the sphere in the solution is of the order 50.0 kT, indicating that the hydrophobic sphere would unlikely escape. Similar conclusion can be drawn for the case of cylindrical particles lying parallel to the bilayer.

IV. CONCLUSIONS

We have developed the SCMF theory for the interaction of nanoscale objects with phospholipid bilayers. This numerical method provides for detailed microscopic information about the structure of phospholipid bilayers and their essential equilibrium thermodynamic properties. The method gives the total equilibrium free energy of self-assembled structures as the output of calculations, which allows for direct comparison of different equilibrium structures involving nanoscale objects and

phospholipid bilayers.

We have applied the SCMF theory to investigate the interaction of phospholipid bilayer with cylindrical and spherical nanoparticles of diameter 2.43 nm and surface properties ranging from hydrophilic to strongly hydrophobic. We have shown that the shape of the nanoparticles is not as important as the contact area with the lipids. Hydrophobic and hydrophilic objects induce different reorganization of lipids around the nanoparticles. More complex nano-objects will be considered in future works.

ACKNOWLEDGMENTS

The authors acknowledge the UK Royal Society International Joint Project with Cambridge University and Spanish Ministry of education MICINN project CTQ2008-06469/PPQ.

[1] Alberts, B. *Molecular Biology of the Cell*, 5th ed.; Garland Science: New York, 2008.

[2] Roiter, Y.; Ornatska, M.; Rammohan, A. R.; Balakrishnan, J.; Heine, D. R.; Minko, S. Interaction of Nanoparticles with Lipid Membrane. *Nanolett.* **2008**, *8*, 941–944.

[3] Wong-Ekkabut, J.; Baoukina, S.; Triampo, W.; Tang, I.-M.; Tieleman, D. P.; Monticelli, L. Computer Simulation Study of Fullerene Translocation Through Lipid Membranes. *Nature Nanotech.* **2008**, *3*, 363–368.

[4] Khodakovskaya, M.; Dervishi, E.; Mahmood, M.; Xu, Y.; Li, Z.; Watanabe, F.; Biris, A. S. Carbon Nanotubes are Able to Penetrate Plant Seed Coat and Dramatically Affect Seed Germination and Plant Growth. *ACS Nano* **2009**, *3*, 3221–3227.

[5] Porter, A. E.; Gass, M.; Muller, K.; Skepper, J. N.; Midgley, P. A.; Welland, M. Direct Imaging of Single-Walled Carbon Nanotubes in Cells. *Nature Nanotech.* **2007**, *2*, 713–717.

[6] Verma, A.; Uzun, O.; Hu, Y.; Hu, Y.; Han, H.-S.; Watson, N.; Chen, S.; Irvine, D. J.; Stellacci, F. Surface-Structure-Regulated Cell-Membrane Penetration By Monolayer-Protected Nanoparticles. *Nature Mat.* **2008**, *7*, 588–595.

[7] Liu, J.; Hopfinger, A. J. Identification of Possible Sources of Nanotoxicity from Carbon Nanotubes Inserted into Membrane Bilayers Using Membrane Interaction Quantitative Structure-Activity Relationship Analysis. *Chem. Res. Toxicol.* **2008**, *21*, 459–466.

[8] Cheng, C.; Muller, K. H.; Koziol, K. K. K.; Skepper, J. N.; Midgley, P. A.; Welland, M. E.; Porter, A. E. Toxicity and Imaging of Multi-Walled Carbon Nanotubes In Human Macrophage Cells. *Biomaterials* **2009**, *30*, 4152–4160.

[9] Venturoli, M.; Sperotto, M. M.; Kranenburg, M.; Smit, B. Mesoscopic Models of Biological Membranes. *Physics Reports* **2006**, *437*, 1–54.

[10] Stewart, K. M.; Horton, K. L.; Kelley, S. O. Cell-Penetrating Peptides As Delivery Vehicles for Biology and Medicine. *Org. Biomol. Chem.* **2008**, *6*, 2242–2255.

[11] Zorko, M.; Langel, U. Cell-penetrating peptides: mechanism and kinetics of cargo delivery. *Adv. Drug Del. Rev.* **2005**, *57*, 529–545.

[12] Bayley, H. Membrane-Protein Structure. Piercing Insights. *Nature* **2009**, *459*, 651–652.

[13] Kafsack, B. F. C.; Pena, J. D. O.; Coppens, I.; Ravindran, S.; Boothroyd, J. C.; Carruthers, V. B. Rapid Membrane Disruption by a Perforin-Like Protein Facilitates Parasite Exit from Host Cells. *Science* **2009**, *323*, 530–533.

[14] Yang, K.; Ma, Y.-Q. Computer Simulation of the Translocation of Nanoparticles with Different Shapes Across a Lipid Bilayer. *Nature Nanotech.* **2010**, *5*, 579–583.

[15] Mouritsen, O. G.; Bloom, M. Mattress Model of Lipid-Protein Interactions In Membranes. *Biophys. J.* **1984**, *46*, 141–153.

[16] Jenssen, H.; Hamill, P.; Hancock, R. E. W. Peptide Antimicrobial Agents. *Clinical Microbiol. Rev.* **2006**, *19*, 491–511.

[17] Monticelli, L.; Salonen, E.; Ked, P. C.; Vattulainen, I. Effects of carbon nanoparticles on lipid membranes: a molecular simulation perspective. *Soft Matter* **2009**, *5*, 4433–4445.

[18] Lopez, C. F.; Nielsen, S. O.; Moore, P. B.; Klein, M. L. Understanding Nature's Design for a Nanosyringe. *Proc. of Nat. Acad. Sci.* **2004**, *101*, 4431–4434.

[19] Bedrov, D.; Smith, G. D.; Davande, H.; Li, L. Passive Transport of C60 Fullerenes through a Lipid Membrane: A Molecular Dynamics Simulation Study. *J. Phys. Chem. B* **2008**, *112*, 2078–2084.

[20] Qiao, R.; Roberts, A. P.; Mount, A. S.; Klaine, S. J.; Ke, P. C. Translocation of C60 and Its Derivatives Across a Lipid Bilayer. *Nano Lett.* **2007**, *7*, 614–619.

[21] Chiu, C.-C.; DeVane, R.; Klein, M. L.; Shinoda, W.; Moore, P. B.; Nielsen, S. O. Coarse-Grained Potential Models for Phenyl-Based Molecules: II. Application to Fullerenes. *J. Phys. Chem. B* **2010**, *114*, 6394–6400.

[22] Pogodin, S.; Baulin, V. A. Can a Carbon Nanotube Pierce through a Phospholipid Bilayer? *ACS Nano* **2010**, *4*, 5293–5300.

[23] Wallace, E. J.; Sansom, M. S. P. Blocking of Carbon Nanotube Based Nanoinjectors by Lipids: a Simulation Study. *Nano Letters* **2008**, *8*, 2751–2756.

[24] Huang, H. W. Molecular Mechanism of Peptide-Induced Pores in Membranes. *Phys. Rev. Lett.* **2004**, *92*, 198304.

[25] Fosnaric, M.; Kralj-Iglic, V.; Bohinc, K.; Iglic, A.; May, S. Stabilization of Pores in Lipid Bilayers by Anisotropic Inclusions. *J. Phys. Chem. B* **2003**, *107*, 12519–12526.

[26] Illya, G.; Deserno, M. Coarse-Grained Simulation Studies of Peptide-Induced Pore Formation. *Biophys. J.* **2008**, *95*, 4163–4173.

[27] Li, Y.; Chen, X.; Gu, N. Computational Investigation of Interaction between Nanoparticles and Membranes: Hydrophobic/Hydrophilic Effect. *J. Phys. Chem. B* **2008**, *112*, 16647–16653.

[28] Nielsen, S. O.; Ensing, B.; Ortiz, V.; Moore, P. B.; Klein, M. L. Lipid Bilayer Perturbations around a Transmembrane Nanotube: A Coarse Grain Molecular Dy-

namics Study. *Biophys. J.* **2005**, *88*, 3822–3828.

[29] Jusufi, A.; DeVane, R. H.; Shinoda, W.; Klein, M. L. Nanoscale Carbon Particles and the Stability of Lipid Bilayers. *Soft Matter* **2011**, *7*, 1139–1146.

[30] Gkeka, P.; Sarkisov, L. Interactions of Phospholipid Bilayers with Several Classes of Amphiphilic alpha-Helical Peptides: Insights from Coarse-Grained Molecular Dynamics Simulations. *J. Phys. Chem. B* **2010**, *114*, 826–839.

[31] Gkeka, P.; Sarkisov, L. Spontaneous Formation of a Barrel-Stave Pore in a Coarse-Grained Model of the Synthetic LS3 Peptide and a DPPC Lipid Bilayer. *J. Phys. Chem. B* **2009**, *113*, 6–8.

[32] Muller, M.; Katsov, K.; Schick, M. Biological and Synthetic Membranes: What Can Be Learned from a Coarse-Grained Description? *Physics Reports* **2006**, *434*, 113–176.

[33] Pogodin, S.; Baulin, V. A. Coarse-Grained Models of Phospholipid Membranes within the Single Chain Mean Field Theory. *Soft Matter* **2010**, *6*, 2216–2226.

[34] Pogodin, S.; Slater, N. K. H.; Baulin, V. A. Surface Patterning of Carbon Nanotubes Can Enhance Their Penetration through a Phospholipid Bilayer. *ACS Nano* **2011**, *5*, 1141–1146.

[35] Rosenbluth, M. N.; Rosenbluth, A. Monte Carlo Calculation of the Average Extension of Molecular Chains. *J. Chem. Phys.* **1955**, *23*, 356–359.